ISSN: 2252-8792, DOI: 10.11591/ijape.v14.i4.pp842-858

Power smoothing in electrical distribution system using covariance matrix adaptation evolution strategy of aquila optimization

Smrutirekha Mahanta, Manoj Kumar Maharana

School of Electrical Engineering, KIIT Deemed to be University, Bhubaneswar, India

Article Info

Article history:

Received Aug 26, 2023 Revised May 19, 2025 Accepted Jun 23, 2025

Keywords:

Aquila optimization CMAES CMAESAO Distribution system FACTS Power smoothing STATCOM

ABSTRACT

This study introduces a novel hybrid optimization approach covariance matrix adaptation evolution strategy of aquila optimization (CMAESAO) to enhance power smoothing and minimize power losses in electrical distribution systems through the optimal allocation of D-STATCOMs. The method is tested on standard 33-bus and 69-bus systems. The CMAESAO algorithm efficiently identifies optimal locations and sizes of D-STATCOMs to achieve system performance improvements under constant power (CP), constant current (CC), and constant impedance (CI) load models. The results show that, for the 69-bus system, installing two D-STATCOMs yields optimal performance, reducing real power loss from the base value to 149.6368 kW, while three D-STATCOMs yield a slightly better voltage profile and VSI but only marginal additional power loss reduction (147.8951 kW), making two units more cost-effective. For the 33-bus system, three D-STATCOMs provide the best improvement in power quality and loss minimization. Voltage and current profiles confirmed improvement in voltage stability and reduced branch currents with optimized placements. Compared to other optimization techniques, CMAESAO demonstrates faster convergence and superior accuracy in minimizing losses, establishing its effectiveness for such multiobjective optimization problems. The study's novelty lies in integrating CMA-ES with aquila optimization to combine strong global search with adaptive exploration, resulting in robust and efficient power system enhancement. The proposed methodology contributes to smarter, more reliable distribution systems, supporting grid resilience and energy efficiency.

This is an open access article under the CC BY-SA license.



842

Corresponding Author:

Smrutirekha Mahanta School of Electrical Engineering, KIIT Deemed to be University Bhubaneswar, Odisha, India Email: m.smrutirekha88@gmail.com

1. INTRODUCTION

Rebuilding of electrical networks was reportedly necessary due to decreasing perishable resource stocks. Renewable energy sources are now integrated into the system as a result of this rebuilding. Over the years, D-STATCOMs have become one of the leaders in the society's current power constraint. The benefits of integrating D-STATCOMs into conventional grids are the most crucial area of study for D-STATCOM location. It enables operators to save back on capital expenditures for managing and improving power systems. It contributes to lowering expenditures for extra control equipment, bolstering transmission and distribution networks, and boosting reliability [1], [2]. Additionally, it helps operators increase efficiency and reduce power transmission loss. The major concerns for a distribution network are it suffers from various issues such as

power losses, poor voltage levels, and limited voltage stability. These problems occur because the system lacks support for reactive power when there is an increase in demand. To overcome these challenges, engineers and researchers have proposed different strategies [3], [4]. Different approaches aim at improving electricity distribution system performance. These techniques consist of establishing voltage regulation mechanisms, incorporating compensating equipment such as shunt capacitors or distributed generators into the network, and adjusting its configuration where necessary [5], [6]. The latest advancements suggest utilizing flexible AC transmission system (FACTS) devices like dynamic voltage regulators (DVRs), D-STATCOMS, and unified power quality conditioners (UPQCs). Among these devices, D-STATCOM is a strong contender due to its ease of connection and local control feature [7]. By connecting D-STATCOM in parallel to the system, it can enhance the profiling of voltage, reduce losses, mitigate issues caused by voltage sags, nonlinear loads, and voltage fluctuations, and increase voltage security margins. In recent years, there has been significant advancement in establishing appropriate strategies for allocating D-STATCOMs more effectively. Sensitivitybased approaches relying on different indicators such as voltage stability index and other related variables are commonly applied today [8], [9]. However, reliance on such methods often poses issues with regard to their reliability. To mitigate this challenge, many researchers have begun exploring alternative methodologies based on metahuristic framework for attaining the optimal allocation of D-STATCOMs. This paper introduces a novel optimization technique (CMAESAO) as a means to determine the allocation D-STATCOMs. A more recent meta-heuristic algorithm, called CMAESAO, is used to optimize allocations of DSTATCOMs [10]. The proposed hybrid CMAESAO technique demonstrates faster convergence, a well-balanced exploration exploitation process, and improved global search ability [11]. Its effectiveness has been validated using 23 benchmark functions, covering various types such as continuous, discontinuous, linear, nonlinear, separable, non-separable, unimodal, and multimodal. The results demonstrated the algorithm's efficiency and reliability in solving optimization problems [12].

2. MODELLING OF ELECTRICAL DISTRIBUTION SYSTEM

Utilizing multiple components such as a voltage source converter, DC capacitor bus, coupling transformer and tuned filter, the D-STATCOM showcases itself as a shunt device worth taking note of while energy storage devices are optional in this device, it's crucial to highlight that deploying voltage source converters enables its ability to function as a generalized impedance converter which permits importing or exporting reactive power at point of common coupling (PCC) [13]. It's noteworthy that when equipped with an energy storage device too, active power injection is within reach. However, the present research only focuses on reactive power regulation for purposes of this study. Figure 1(a) illustrates a two-bus equivalent of the distribution network for [14].

$$V_{t+1} \angle \theta_{t+1} = V_t \angle \theta_t - (R_m + jX_m) \angle \delta_m \tag{1}$$

The compensated network, along with the DSTATCOM configuration and the phasor representation of the compensation network as described in (1) and (2), is illustrated in Figure 1(b).

$$V_{t+1} \angle \theta_{t+1} = V_t \angle \theta_t - (R_m + jX_m)(I_m D\delta_m + I_{Dstatcom} + \psi)$$
(2)

Since the D-STATCOM functions as a reactive power source, its current is phase-shifted by 90 degrees with respect to the voltage at the compensated node. Consequently, it injects or absorbs reactive power without affecting the active power flow, thereby improving voltage stability and power quality at the point of connection.

$$\psi = \frac{\pi}{2} + \theta'_{t+1} \tag{3}$$

The power injected by the D-STATCOM can be expressed as (4).

$$-jQ_{Dstatcom} = V'_{t+1} \angle \theta'_{t+1} + I''_{Dstatcom} \angle \left(\frac{\pi}{2} + \theta'_{t+1}\right)$$

$$\tag{4}$$

This research employs the covariance matrix adaptation evolution strategy of aquila optimization to determine the optimal locations and capacities of multiple D-STATCOMs, aiming to minimize active (real) power loss in the electrical distribution system. The optimization process adheres to operational constraints outlined in (3) and (4). Since distribution utilities prioritize reducing real power loss due to its direct economic impact more so than voltage regulation or system stability [15]. The primary objective of this research is the optimal

844 🗖 ISSN: 2252-8792

allocation of D-STATCOMs to achieve minimal real power loss. Mathematically, the real power loss is expressed in (5).

$$P_{loss} = \sum_{m=1} |I_m|^2 \times R_m \tag{5}$$

The primary objective is to minimize real power loss in the distribution system, which is formulated as the objective function presented in (6).

$$O_F = \min(P_{loss}) = \min(\sum_{m=1}^{\infty} |I_m|^2 \times R_m)$$
(6)

The network's bus voltage is permitted to vary within a range of $\pm 5\%$ of the nominal voltage. The current flow within the distribution network is certainly to be affected by the presence of DSTATCOM. Therefore, a constraint is established to restrict the branch flow within the prescribed limits when D-STATCOMs are introduced. The nodes used for insertion of DSTATCOMs are not prone to repetition. The size of allocated DSTATCOMs must be bound by (7).

$$\sum_{i=1} QDstatcom, i = \sum_{t=1} Qload, t$$
(7)

The allocation of DSTATCOMs is optimized through the use of CMAESAO. It is a combination of the benefits of two optimization techniques are CMAES and AO [16].

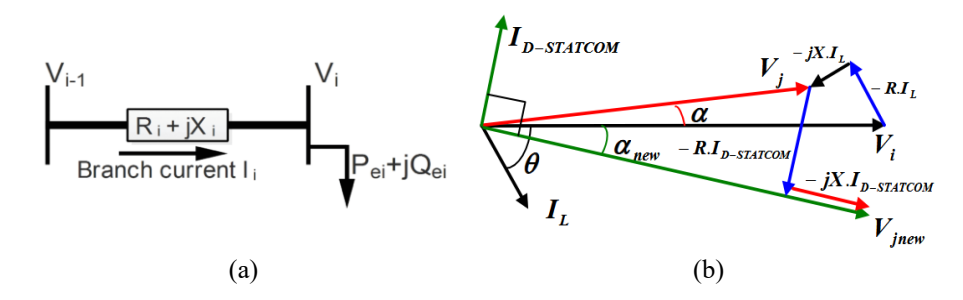


Figure 1. DSTATCOM compensation in a distribution network: (a) two-bus equivalent of the distribution network and (b) phasor diagram of DSTATCOM

3. COVARIANCE MATRIX ADAPTATION EVOLUTION STRATEGY

Covariance matrix adaptation evolution strategy (CMA-ES) is a powerful evolutionary algorithm designed for continuous domain optimization problems. It is particularly effective for non-linear, non-convex, and ill-conditioned optimization tasks where gradient-based methods may struggle or fail. The core idea of CMA-ES is to evolve a population of candidate solutions by sampling from a multivariate normal distribution, that mean and covariance matrix are updated iteratively to reflect the topology of the objective function. At each generation, new candidate solutions (offspring) are sampled from a Gaussian distribution centered around the current mean. The covariance matrix plays a critical role in shaping this distribution, allowing the algorithm to capture dependencies between variables and adapt the search direction. The best-performing individuals, based on the fitness function, are selected, and the distribution parameters (mean, step size, and covariance matrix) are updated accordingly. The most distinguishing feature of CMA-ES is the covariance matrix adaptation. This mechanism enables the algorithm to learn the shape of the objective function landscape dynamically. Over time, the covariance matrix reflects the correlation structure between variables, guiding the sampling process toward promising regions in the search space. The algorithm also includes mechanisms such as step-size control and evolution paths to improve convergence and exploration-exploitation balance. CMA-ES does not require gradient information, making it well-suited for black-box optimization problems. It has been successfully applied in various domains, including machine learning model tuning, control systems, robotics, and engineering design. Despite its computational cost due to covariance matrix updates, its robustness and self-adaptation capabilities make it one of the most reliable evolutionary strategies for challenging optimization problems. The (8) represents the updated evolution.

$$m_{new} = m_{old} \times p_{step} \tag{8}$$

Where, m_{new} , m_{old} , and p_{step} denotes new mean, old mean, and the evolution path, respectively. The adaptation for σ is expressed by (9).

$$\sigma_{new} = \sigma_{old} \times exp\left(\frac{c_{\sigma}}{d_{\sigma}} \left(\frac{\|P_{step}\|}{E\|N(0,I)\|} - 1\right)\right)$$
(9)

Where, σ_{new} , σ_{old} , c_{σ} , d_{σ} , E, and N(0,I) represents the new step-size, old step size, normalization constant, damping parameter, expected value, and expected length to update the conjugate evolution path, respectively. The adaptation for C is expressed by (10).

$$C_{new} = (1 - c_1 - c_\mu) \times C_{old} + c_1 \times (P_{step} \times P_{step}^T) + c_\mu \times \sum_{i=1}^{\mu} \omega_i \times (y_i \times y_i^T)$$
 (10)

Where, C_{new} , c_1 , c_μ , C_{old} , P_{step}^T , ω_i , y_i , and y_i^T represents the new covariance matrix, update parameter-1, update parameter-2, old covariance matrix, conjugate of the evolution path, weight assigned to each solution candidate, weighted difference vector of solution, and its conjugate, respectively [17].

Figure 2 presents the flowchart for the covariance matrix adaptation evolution strategy (CMAES) technique, illustrating its iterative optimization process. The algorithm begins with the initialization of key parameters such as population size, mean vector, and covariance matrix. It then enters a loop where a new population of candidate solutions is sampled from a multivariate normal distribution [18]. These solutions are evaluated using a fitness function, and the best-performing individuals are selected to update the mean and covariance matrix, effectively guiding the search towards promising regions in the solution space. The process continues iteratively, adapting step sizes and covariance to improve convergence until a stopping criterion, such as a maximum number of generations or convergence threshold, is met [19].

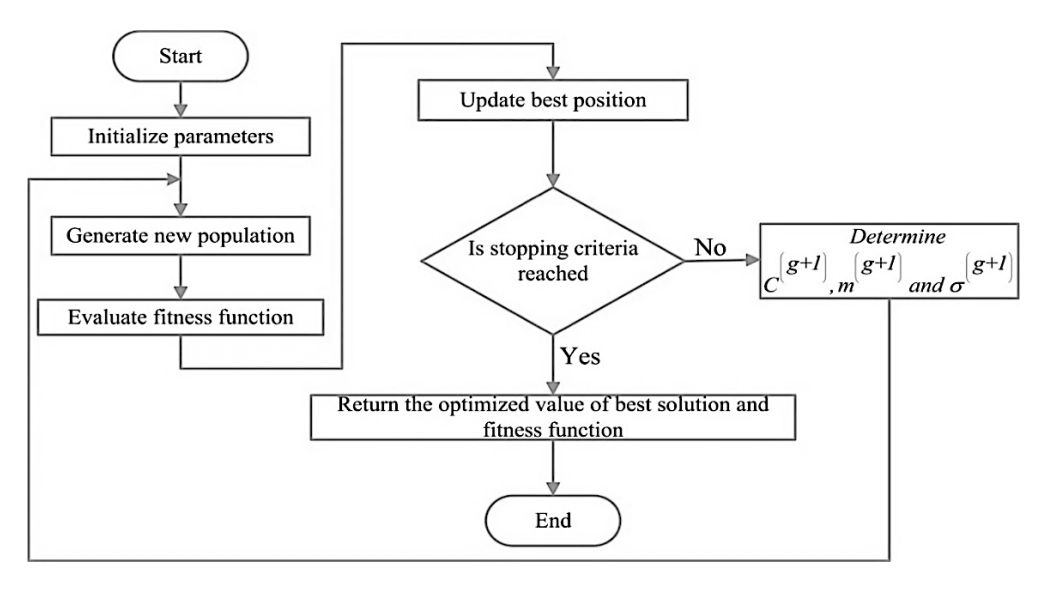


Figure 2. Flowchart for CMAES technique

4. AQUILA OPTIMIZATION (AO)

Aquila optimization (AO) is a recent nature-inspired metaheuristic algorithm that mimics the intelligent hunting strategies of the aquila (eagle). This bird of prey uses four distinct methods—high soar with vertical stoop, contour flight with glide attack, low flight with slow descent, and walk-and-grab—to adaptively catch its prey, depending on the target's location and movement. Similarly, AO models the exploration and exploitation phases of optimization based on these hunting strategies, enabling it to switch dynamically between global and local searches during the problem-solving process. In the AO algorithm, the optimization begins by initializing a population of candidate solutions. The total number of candidates is denoted by N, and each candidate operates within a solution space defined by the dimension D. These candidates form a two-dimensional array X of size N×D times N×D, where each row represents a potential solution. The initial positions are randomly generated within the defined boundaries of the problem. AO then applies one of the four modeled hunting behaviors based on a probabilistic selection mechanism, which is mathematically

governed by (13), allowing the algorithm to balance exploration and exploitation effectively. As the iterations progress, each candidate's position is updated according to the strategy selected in that iteration. The performance or fitness of each candidate is evaluated using a problem-specific fitness function. The best candidate is preserved across generations, and the population adapts accordingly. AO's adaptability and strategic update mechanism enable it to converge quickly to the global optimum while avoiding local minima, making it suitable for solving complex optimization problems in various engineering and computational domains [20].

Figure 3 illustrates the flowchart for the aquila optimization (AO) algorithm, depicting its structured approach to solving complex optimization problems. The process begins with the initialization of key parameters, including the number of candidate solutions, dimensionality of the problem space, and boundary constraints. An initial population of potential solutions is randomly generated and evaluated using a defined fitness function. The best solution among them is identified and stored for reference [21]. Based on a random probability and the current iteration, the algorithm selects one of the four aquila-inspired hunting strategies to guide the movement of candidates ranging from global soaring and gliding to precise local attacks. In the iterative loop, each candidate solution is updated based on the selected strategy, reflecting the dynamic nature of aquila's hunting behavior [22]. These strategies balance exploration (searching new areas) and exploitation (refining known good solutions). After each update, the fitness of the new candidates is evaluated, and the best solution is updated if a superior one is found [23]. This process repeats until a termination criterion, such as reaching the maximum number of iterations or achieving a satisfactory fitness level, is met. The flowchart effectively captures the adaptive and intelligent nature of AO, showcasing how it emulates aquila's flexible hunting tactics to navigate the search space and find optimal solutions [24].

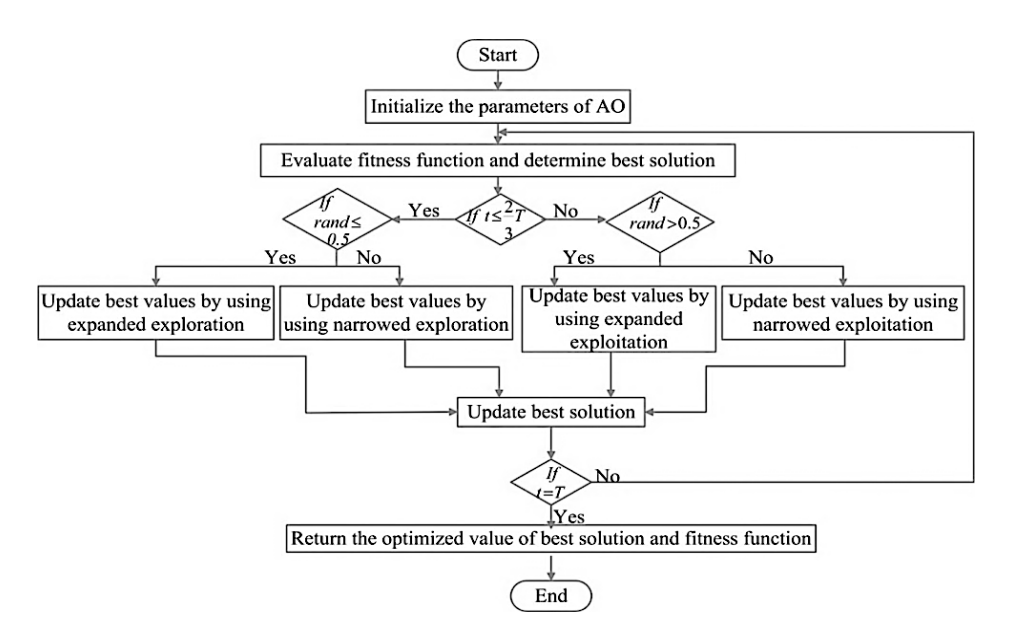


Figure 3. Flowchart for AO

5. COVARIANCE MATRIX ADAPTATION EVOLUTION STRATEGY BASED AQUILA OPTIMIZATION

The covariance matrix adaptation evolution strategy-based aquila optimization (AOCMAES) is a novel hybrid algorithm that combines the strengths of two powerful optimization techniques aquila optimization (AO) and covariance matrix adaptation evolution strategy (CMAES). AO is known for its efficient global search capabilities inspired by the hunting strategies of aquila eagles. However, despite its exploratory strength, AO often suffers from slower convergence, longer runtimes, and a tendency to get trapped in local optima when dealing with complex problem landscapes. To overcome these limitations, the proposed AOCMAES integrates the local search efficiency of CMAES into the AO framework. CMAES, as a local optimizer, adapts the covariance matrix of a multivariate normal distribution to guide the generation of new candidate solutions [25]. It excels in fine-tuning solutions by exploiting the search space around promising regions, leading to faster convergence and improved precision. By embedding CMAES into AO's iteration cycle, the hybrid algorithm benefits from both the exploration ability of AO and the exploitation efficiency of CMAES. This integration helps in escaping local optima and achieving global optima more consistently and

quickly [26]. In AOCMAES, the optimization begins with AO's global search phase, where diverse candidate solutions explore the wider search space. When the algorithm identifies a promising region or begins to stagnate, the CMAES module is triggered to perform an intensive local search around the best solution. This dynamic switching ensures that the exploration is not prematurely stopped and that the algorithm can fine-tune optimal solutions effectively. The balance between exploration and exploitation is thereby significantly enhanced [27]. Overall, the AOCMAES hybrid algorithm delivers superior optimization performance by combining the global reach of AO and the local precision of CMAES. The result is an improved convergence rate, reduced computation time, and enhanced robustness in navigating complex search spaces. The optimization parameters are adaptively tuned during the run to ensure that the algorithm approaches optimal solutions within a shorter interval, making it suitable for real-world engineering and computational applications requiring high efficiency and accuracy [28].

Figure 4 illustrates the numerical representation of key optimization parameters used in the CMAESAO technique through a bar graph. The graph shows that the maximum number of iterations is set to 1000, highlighting the algorithm's capacity for extensive searching [29]. Both the alpha (α) and delta (δ) parameters, which control the exploration and exploitation balance, are set to their average values of 0.5 within the range [0.1, 0.9]. The problem dimensionality is relatively low at 4, indicating a moderate complexity of the search space. Lastly, the number of aquilas (candidate solutions) is 100, reflecting a robust population size to support diverse global search capabilities. This visualization helps in understanding the scale and role of each parameter in the optimization process [30].

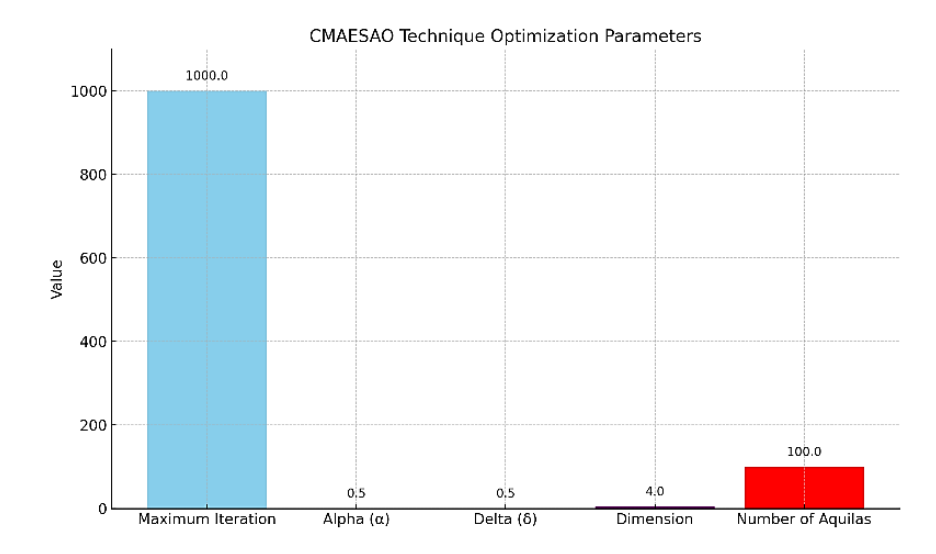


Figure 4. Parameters for CMAESAO

Figure 5 presents the flowchart for the covariance matrix adaptation evolution strategy-based aquila optimization (CMAESAO) technique, depicting the integration of AO and CMAES for enhanced optimization performance. The process initiates with the input of algorithm-specific parameters such as population size (number of aquilas), dimension of the problem space, alpha (α), delta (δ), and the maximum number of iterations. An initial population of candidate solutions is generated randomly within the defined bounds, and each solution's fitness is evaluated using a predefined objective function. The best solution is identified and stored for future reference [31]. Following initialization, the main optimization loop begins, where the aquila optimization (AO) strategies are applied to guide global search. These strategies mimic different hunting behaviors of Aquilas and allow candidates to explore diverse regions of the solution space. Based on a selection mechanism influenced by α and δ , the algorithm decides whether to perform exploration or move towards exploitation. When stagnation or promising regions are detected, the CMAES module is triggered. CMAES then conducts a focused local search using adaptive multivariate normal sampling, updating the mean and covariance matrix to refine the solution around the best candidate. This hybrid process continues iteratively, with the algorithm alternating between AO's global search and CMAES's local refinement based on convergence behavior [32]. At each step, the population is updated, and the fitness of new candidates is compared to identify improvements. The loop terminates when the maximum number of iterations is reached or an acceptable solution is found. The flowchart in Figure 4 clearly outlines the intelligent switching and cooperation between AO and CMAES, illustrating how their synergy results in improved convergence speed, reduced computational effort, and more reliable global optimization outcomes [33].

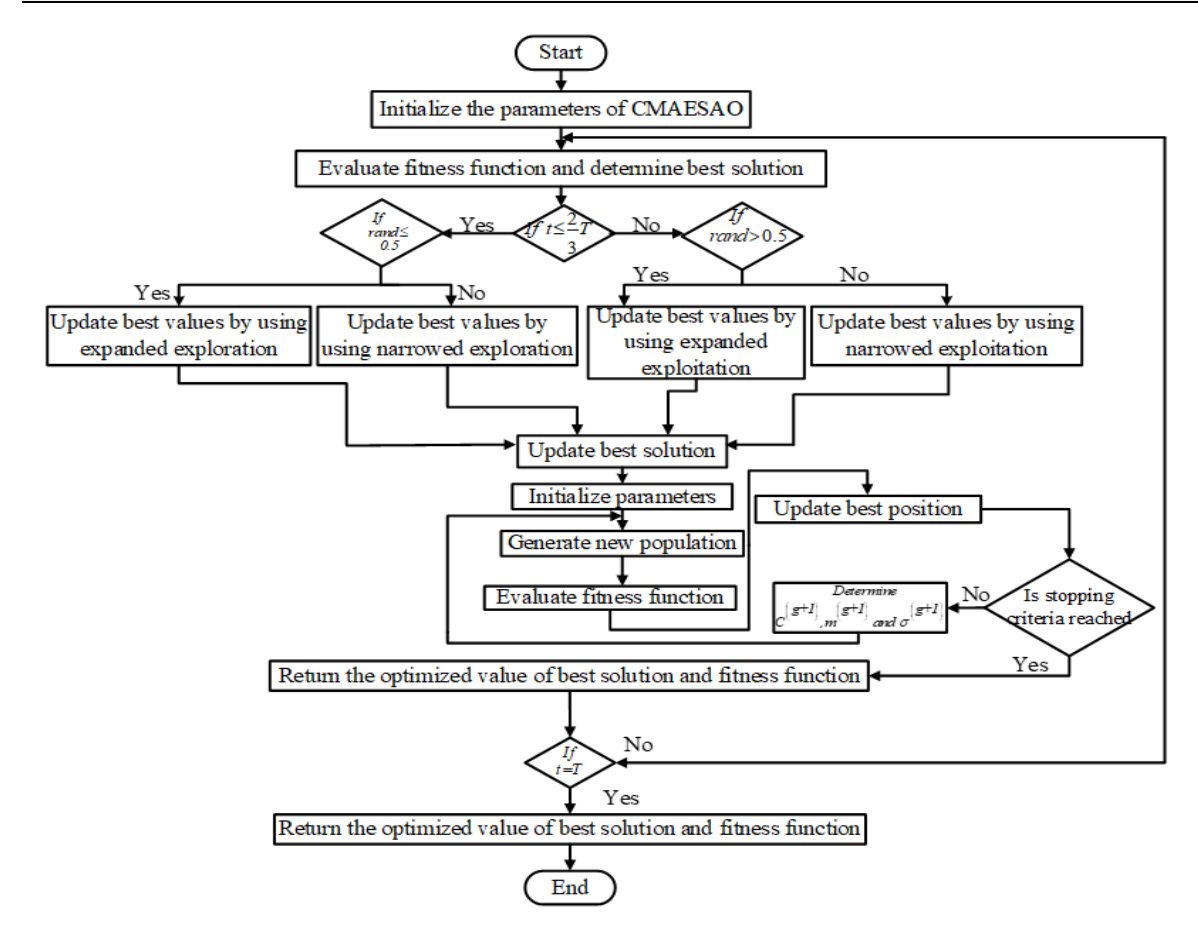


Figure 5. CMAESAO technique flowchart algorithm

6. RESULTS AND DISCUSSION

The performance of the proposed CMAESAO technique has been rigorously evaluated using a comprehensive set of benchmark functions. Table 1 presents the details of these benchmark functions, which include a diverse range of mathematical test problems commonly used in optimization research. These functions vary in complexity, modality (unimodal or multimodal), dimensionality, and landscape characteristics, making them ideal for assessing the robustness and versatility of the optimization algorithm. They test an optimizer's ability to locate global optima, escape local minima, and converge efficiently across different search landscapes. In this study, a total of 23 benchmark functions, as outlined in Table 1have been employed to validate the effectiveness of the CMAESAO hybrid technique. These include well-known functions such as Sphere, Rastrigin, Ackley, Griewank, and Rosenbrock, among others. By comparing the results of CMAESAO with standard optimization algorithms, the study demonstrates its superior convergence rate, higher solution accuracy, and stronger balance between exploration and exploitation. The wide variety of benchmark functions ensures that the performance evaluation is comprehensive and realistic, ultimately proving the hybrid algorithm's capability to handle diverse and complex optimization tasks efficiently.

Table 1 outlines the comprehensive set of benchmark functions used to evaluate the performance of the proposed CMAESAO algorithm. These functions span a wide range of optimization landscapes, including unimodal and multimodal functions, making them suitable for assessing both exploration and exploitation capabilities. Each function is tested in a specified dimensional space—mostly 30 dimensions, except for a few lower-dimensional functions (e.g., 2D, 3D, 4D, and 6D) to reflect real-world problems with varying complexity. The functions operate within defined input ranges, such as [-100,100][-100, 100][-100,100], [-600,600][-600,600][-600,600], or [0,1][0, 1][0,1], which influence the difficulty level of locating global optima. These benchmark functions include widely studied mathematical formulations such as Sphere, Rastrigin, Ackley, Rosenbrock, and Griewank functions, among others. They are known for their varied characteristics like high non-linearity, ruggedness, deceptive local minima, and sharp valleys. By including such a diverse set, the evaluation tests how efficiently CMAESAO navigates through different types of objective surfaces. This range of functions ensures that the algorithm is not biased toward specific problem types and maintains generalizability across optimization scenarios. The performance of CMAESAO has been

further compared against a broad array of established metaheuristic algorithms including grasshopper optimization algorithm (GOA), equilibrium optimization (EO), particle swarm optimization (PSO), dragonfly algorithm (DA), ant lion optimization (ALO), grey wolf optimizer (GWO), marine predator algorithm (MPA), salp swarm algorithm (SSA), sine cosine algorithm (SCA), whale optimization algorithm (WOA), and slime mould algorithm (SMA). Each of these algorithms has proven effective in different studies, yet the hybrid CMAESAO has demonstrated enhanced robustness and convergence consistency across all benchmark cases.

Table 2 presents the detailed performance comparison between the standalone aquila optimization (AO) and the hybrid CMAESAO algorithm using various benchmark functions. For each function, metrics such as mean, standard deviation, best, and worst values were computed across multiple runs to assess consistency, accuracy, and robustness. The first major observation is the substantial improvement in convergence precision achieved by CMAESAO. For example, in functions where AO already produced extremely small mean values (in the order of 10⁻²¹⁸, CMAESAO pushed performance even further into the range of 10^{-266} , showcasing its superior ability to approach global optima with higher precision and stability. The comparison also highlights CMAESAO's remarkable advantage in standard deviation values, which remain significantly lower or even zero in many cases, indicating high consistency and minimal variation in outcomes. This is especially evident in functions involving multimodal landscapes, where AO tends to show noticeable variance between best and worst cases. In contrast, CMAESAO maintains tight performance bounds, proving its robustness. For example, in one of the benchmark functions, AO's worst-case result is several magnitudes higher than its best, while CMAESAO remains tightly clustered around optimal performance with negligible standard deviation. The CMAESAO outperforms AO in best and worst-case scenarios, indicating better reliability in extreme outcomes. For instance, in several benchmark cases, CMAESAO's worst performance is still significantly better than AO's best. This illustrates the hybrid model's capability to avoid poor local optima and navigate complex search spaces more effectively. The inclusion of CMAES enhances local exploitation, fine-tuning the solutions identified by AO's broader global exploration mechanisms. Overall, the results in Table 2 validate the effectiveness of the CMAESAO hybrid approach across diverse benchmark functions. It consistently surpasses AO in all statistical metrics, including mean accuracy, variance control, and extremum performance. The integration of CMAES ensures not only faster convergence but also a more precise and reliable optimization process. This performance gain confirms the hybrid algorithm's suitability for solving high-dimensional and computationally challenging optimization problems in real-world applications.

6.1. Performance index using statistical analysis

The statistical analysis of the performance index highlights the enhanced efficiency of the proposed CMAESAO algorithm by directly comparing it with the original AO under identical conditions. Both algorithms were subjected to the same fitness function f(x) and evaluated using identical optimization parameters, ensuring a fair and consistent comparison. The analysis focused on key performance indicators such as the integral of time-weighted absolute error (ITAE), which is widely used to assess convergence quality and control precision. As seen in Figure 5, CMAESAO consistently outperforms AO by achieving significantly lower ITAE values, indicating faster and more accurate convergence toward optimal solutions.

Moreover, the results reveal that CMAESAO exhibits less variation in performance across multiple runs, reflected by its reduced standard deviation. This consistency indicates the hybrid algorithm's robustness and reliability in handling complex optimization landscapes. The integration of CMAES into the AO framework improves local exploitation, enabling precise fine-tuning of solutions after initial global exploration. As a result, CMAESAO not only reaches optimal solutions more efficiently but also does so with greater repeatability and minimal deviation, validating its statistical superiority over standalone AO.

Figure 6 presents a plot of the integral of time-weighted absolute error (ITAE) values versus the number of runs for both the AO and CMAESAO algorithms, clearly demonstrating the superior performance of CMAESAO. The blue line representing AO shows higher ITAE values with significant fluctuations across the 30 runs, indicating inconsistent performance and higher error. In contrast, the red line representing CMAESAO remains consistently lower and more stable, with ITAE values clustered around 0.48–0.50. This highlights CMAESAO's robustness, reduced deviation, and improved control performance, confirming its reliability and efficiency in producing optimal solutions with minimal error across multiple iterations.

The graphical analysis in Figure 7 illustrates the statistical comparison of AO and CMAESAO clearly highlights the superior performance of the CMAESAO algorithm across all four statistical metrics. The blue bars representing the AO algorithm show significantly higher values in terms of maximum, minimum, and mean ITAE, along with a much larger standard deviation. In contrast, the red bars representing CMAESAO are consistently lower across all categories. Notably, CMAESAO's maximum ITAE (0.5021) is even lower than AO's minimum (0.6007), indicating a drastic reduction in error and variability. This visual evidence strongly supports the claim that CMAESAO provides a more stable, reliable, and accurate optimization solution. The standard deviation for CMAESAO is extremely low (0.0079), compared to AO's 0.0568,

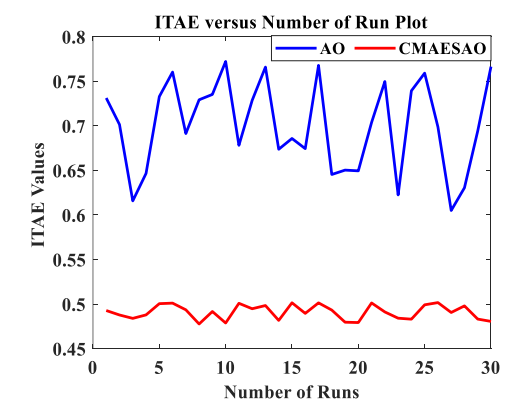
demonstrating that CMAESAO not only delivers better results on average but also ensures consistency across multiple runs. This makes CMAESAO an ideal choice for applications requiring high precision and dependable convergence behavior.

Table 1 Performance analysis of CMAESAO benchmark functions

	Table 1. Performance analysis of CMAESAO bend	chmark function	ns	
Function name	Function definition	Dimension (D)	Range	F_{min}
$F_1(x)$	$F_1(x) = \sum_{i=1}^D x_i^2$	30	[-100,100]	0
$F_2(x)$	$F_2(x) = \sum_{i=0}^{D} x_i + \prod_{i=0}^{D} x_i $	30	[-10,10]	0
$F_3(x)$	$F_3(x) = \sum_{i=1}^{D} (\sum_{i=1}^{i} (x_i))^2$	30	[-100,100]	0
$F_4(x)$	$F_4(x) = \max_i \max\{ x_i , (1 \le i \le n)\}$	30	[-100,100]	0
$F_5(x)$	$F_5(x) = \sum_{i=1}^{D} [100(x_i^2 - x_{i+1})^2 + (1 - x_i)^2]$	30	[-30,30]	0
$F_6(x)$	$F_6(x) = \sum_{i=1}^{D} ([x_i + 0.5]^2)$	30	[-100,100]	0
$F_7(x)$	$F_7(x) = \sum_{i=1}^{D} \left(i \times x_i^4 + random(0,1) \right)$	30	[-128,128]	0
$F_8(x)$	$F_8(x) = \sum_{i=1}^{D} \left(-x_i \sin\left(\sqrt{ x_i }\right) \right)$	30	[-500,500]	0
		30	[-5.12, 5.12]	-418.9829
$F_9(x)$	$F_9(x) = \sum_{i=1}^{D} (x_i^2 - 10\cos(2\pi x_i) + 10)$			$\times D$
$F_{10}(x)$	$F_{10}(x) = -20 \times exp\left(-0.2\sqrt{\frac{1}{D}\sum_{i=1}^{D}x_i^2}\right) -$	30	[-32,32]	0
	$exp\left(\frac{1}{D}\sum_{i=1}^{D}cos(2\pi x_i)\right) + 20 + e$			
$F_{11}(x)$	$F_{11}(x) = 1 + \frac{1}{4000} \sum_{i=1}^{D} x_i^2 - \prod_{i=1}^{D} \cos\left(\frac{x_i}{\sqrt{i}}\right)$	30	[-600,600]	0
$F_{12}(x)$	$F_{12}(x) = \frac{\pi}{n} \{10sin(\pi y_i)\}$ $+ \sum_{i=1}^{D-1} (y_i - 1) \left[1 + 10sin^2(\pi y_{i+1}) + \sum_{i=1}^{D} u(x_i, 10, 100, 4) \right]$ $where, u(x_i, a, k, m) = \begin{cases} K(x_i - a)^m & \text{if } x_i > a \\ 0 & -a \pounds x_i > a \end{cases};$ $y_i = 1 + \frac{1 + x_i}{4};$	30	[-50,50]	0
$F_{13}(x)$	$F_{13}(x) = 0.1sin^{2}(3\mu x1) + \sum_{i=1}^{D} (x_{i} - 1)^{2}[1 + sin^{2}(3\mu x_{i} + 1)] + (xD - 1)^{2} + sin^{2}(2\mu xD) + \sum_{i=1}^{D} (x_{i}, 5, 100, 4)$	30	[-50,50]	0
$F_{14}(x)$	$F_{14}(x) = \left(\frac{1}{500} + \sum_{j=1}^{25} \frac{1}{j + \sum_{i=1}^{2}} (x_i - a_{ij})\right)^{-1}$	2	[-65,65]	0
	2	4	[-5,5]	0
$F_{15}(x)$	$F_{15}(x) = \sum_{i=1}^{11} \left[a_i - \frac{x_1(b_i^2 + b_i x_2)}{(b_i^2 + b_i x_3 + x_4)} \right]^2$			
$F_{16}(x)$	$F_{16}(x) = 4x_1^2 - 2.1x_1^4 + \frac{1}{2}x_1^6 + x_1x_2 - 4x_2^2 + 4x_2^4$	2	[-5,5]	0
$F_{17}(x)$	$F_{17}(x) = \left(x_2 - \frac{5.1}{4\pi^2}x_1^2 + \frac{5}{\pi}x_1 - 6\right)^2 + 10\left(1 - \frac{1}{8\pi}\right)\cos x_1 + 10$	2	[-5,5]	0
	$F_{18}(x) = \begin{bmatrix} 1 + (x_1 + x_2 + 1)^2 (19 - 14x_1 + 3x_2 1 - 14x_2 + 6x_1x_2 + 3x_2^2) \end{bmatrix}$	2	[-2,2]	0
$F_{18}(x)$ $F_{19}(x)$	$ \begin{aligned} \times \left[30 + (2x_1 - 3x_2)^2 \times (18 - 32x_i + 12x_1^2 + 48x_2 - 36x_1x_2 + 27x_2^2) \right] \\ + 12x_1^2 + 48x_2 - 36x_1x_2 + 27x_2^2) \right] \\ F_{19}(x) &= -\sum_{i=1}^4 c_i exp \left(-\sum_{j=1}^3 a_{ij} (x_j - p_{ij})^2 \right) \end{aligned} $	3	[-1,2]	0
$F_{20}(x)$	$F_{20}(x) = -\sum_{i=1}^{4} c_i exp \left(-\sum_{j=1}^{6} a_{ij} (x_j - p_{ij})^2 \right)$	6	[0,1]	0
$F_{21}(x)$	$F_{21}(x) = -\sum_{i=1}^{5} [(X - a_i)(X - a_i)T + c_i]$	4	[0,1]	0
$F_{22}(x)$	$F_{22}(x) = -\sum_{i=1}^{7} [(X - a_i)(X - a_i)T + c_i]$	4	[0,1]	0
$F_{23}(x)$	$F_{23}(x) = -\sum_{i=1}^{10} [(X - a_i)(X - a_i)T + c_i]$	4	[0,1]	0

Table 2. Performance evaluation of CMAESAO and AO

	Table 2	Performan	ice evaluatio	n of CMAESA	O and AO		
Function name	Metrics	AO	CMAESAO	Function name	Metrics	AO	CMAESAO
	Mean	9.4973e ⁻²¹⁸	6.23e ⁻²⁶⁶		Mean	$2.3207e^{0}$	0.0068
	Standard Deviation	$0.00e^{000}$	$0.00e^{000}$		Standard	$1.0246e^{0}$	$9.3403e^{-13}$
$F_2(x)$				$F_{14}(x)$	Deviation		
	Best	6.5477e ⁻²²⁵	1.2406e ⁻²⁶⁸		Best	9.9800e1	1.565e ⁻⁰⁴
	Worst	3.214e ⁻²¹⁷	6.2425e ⁻²⁶⁵		Worst	2.9821e0	0.0274
	Mean	9.9112e ⁻²¹⁸	8.8368e ⁻²⁵¹		Mean	5.5089e-4	1.2106e ⁻⁵⁸
	Standard Deviation	$0.00e^{000}$	$0.00e^{000}$		Standard	1.9027e-4	3.7682e ⁻⁵⁸
$F_4(x)$				$F_{15}(x)$	Deviation		
* ' '	Best	2.322e ⁻²¹¹	3.5950e ⁻²⁴⁷	13 ,	Best	4.0581e-4	7.6985e ⁻⁶²
	Worst	3.4546e ⁻²¹⁷	1.7427e ⁻²⁴⁵		Worst	8.4575e-4	9.6548e ⁻⁵⁸
	Mean	1.8851e ⁻³	$0.00e^{000}$		Mean	-1.0316	-3.7895e ⁻⁰³
	Standard Deviation	2.5151e ⁻³	$0.00e^{000}$		Standard	6.5206e-8	1.1659e ⁻¹⁸
$F_5(x)$				$F_{16}(x)$	Deviation		
3()	Best	5.8588e ⁻⁵	$0.00e^{000}$	10 ()	Best	-1.0316	-3.7895e ⁻⁰³
	Worst	2.5151e ⁻³	$0.00e^{000}$		Worst	-1.0316	-5.6879e ⁻⁰¹
	Mean	6.3114e ⁻⁵	1.2858e ⁻⁰⁵		Mean	3.9789e-1	$0.4208e^{-3}$
	Standard Deviation	2.9614e ⁻⁵	1.2809e ⁻⁰⁷		Standard	4.7081e-7	1.0600e ⁻¹⁵
$F_6(x)$				$F_{17}(x)$	Deviation		
000	Best	7.28e ⁻⁸	1.1399e ⁻⁶	17 (-7	Best	3.9789e-1	$0.4208e^{-3}$
	Worst	1.9689e ⁻⁴	2.4937e ⁻⁵		Worst	3.9789e-1	$0.4208e^{-3}$
	Mean	1.5929e ⁻³	7.9575e ⁻⁰⁵		Mean	-3.8624	-0.3926
	Standard Deviation	4.8479e ⁻⁴	6.9694e ⁻⁰⁴		Standard	8.4657e-4	9.6523e ⁻⁵
$F_7(x)$				$F_{19}(x)$	Deviation		
/ \ /	Best	6.6048e ⁻⁵	1.6114e ⁻⁴	19 ()	Best	-3.8628	-0.3926
	Worst	1.5929e ⁻³	1.5365e ⁻⁰⁴		Worst	-3.8607	-0.3926
	Mean	$-2.2694e^{3}$	$-1.8025e^{3}$		Mean	-3.3014	-5.4250
	Standard Deviation	$4.6187e^{2}$	8.4242		Standard	4.9969e ⁻²	$7.8695e^{-3}$
$F_8(x)$				$F_{20}(x)$	Deviation		
0 ()	Best	$-2.6958e^{3}$	$-1.80247e^{3}$	20(**)	Best	-3.3220	-5.7693
	Worst	$1.4073e^{3}$	$-1.80247e^{3}$		Worst	-3.1994	-5.7673
	Mean	8.8818e ⁻¹⁶	9.1595e ⁻¹⁷		Mean	-10.149	-10.1413
	Standard Deviation	0.00e000	0.00e000		Standard	4.9969e ⁻²	4.8699e ⁻²
$F_{10}(x)$				$F_{21}(x)$	Deviation		
- 10 (00)	Best	8.8818e ⁻¹⁶	1.6438e ⁻¹⁶	- 21(**)	Best	-10.153	-10.1413
	Worst	8.8818e ⁻¹⁶	1.6438e ⁻¹⁶		Worst	-10.14	-10.1413
	Mean	2.9262e ⁻⁵	1.3676e ⁻⁰⁷		Mean	-10.401	-10.3801
	Standard Deviation	3.5700e ⁻⁵	1.4126e ⁻⁰⁷		Standard	2.9768e ⁻³	2.8765e ⁻³
$F_{12}(x)$	Standard Deviation	3.07000	11.11200	$F_{22}(x)$	Deviation	213 7 000	2.07020
112(11)	Best	1.1309e ⁻⁷	5.7279e ⁻⁰⁹	1 22(21)	Best	-11.040	-10.3801
	Worst	1.0421e ⁻⁴	3.7378e ⁻⁰⁷		Worst	-10.395	-10.3801
	Mean	9.5026e ⁻⁵	6.0499e ⁻⁰⁷		Mean	-10.536	-10.535
	Standard Deviation	1.0312e ⁻⁴	3.8953e ⁻⁰⁸		Standard	2.756e-4	2.755e-4
$F_{13}(x)$	Samura Deviation	1.03120	3.0733 c	$F_{23}(x)$	Deviation	2.7500 4	2.7330 7
- 13(~)	Best	2.7176e ⁻⁶	7.77564e ⁻⁰⁶	- 23 (~)	Best	-10.536	-10.535
	Worst	2.7104e ⁻⁴	2.0815e ⁻⁰⁵		Worst	-10.535	-10.534
	WOIST	2./10 4 0	2.00136		WOISt	-10.555	-10.554



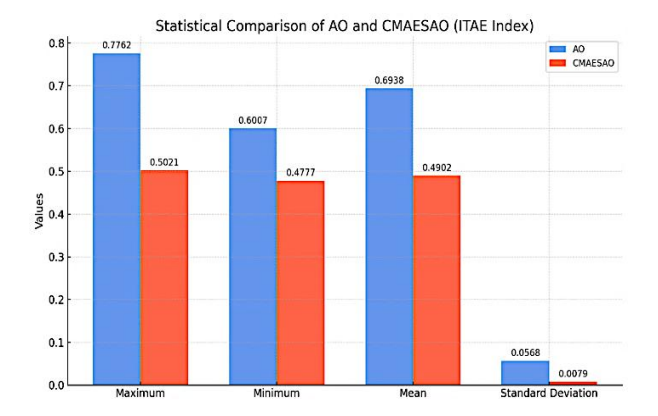


Figure 6. ITAE versus no runs plot

Figure 7. Statistical comparison of AO and CMAESAO

6.2. Convergence rate analysis

Figure 8 presents the convergence plot of ITAE values over the number of iterations for both the AO and CMAESAO algorithms, showcasing their optimization performance. The blue crosses represent AO, which starts with higher ITAE values and gradually reduces over time but plateaus early, showing slower and less

stable convergence. In contrast, the red diamonds representing CMAESAO display a much faster and smoother convergence path. A focused inset between iterations 50 and 75 reveals that CMAESAO consistently outperforms AO throughout the iterative process, with lower ITAE values at nearly every step.

It is clearly observed from Figure 8 that AO converges prematurely around an ITAE value of 0.7067, while CMAESAO continues to optimize and reaches a significantly better minimum of 0.4779. Although AO appears to converge earlier, it stabilizes at a suboptimal value. This demonstrates that while AO settles quickly, it lacks the precision and depth to reach the global optimum effectively. CMAESAO, on the other hand, maintains a controlled and steady optimization path, leading to superior results. This performance gain confirms the advantage of integrating CMAES into AO, improving convergence quality and solution accuracy significantly over the standard AO algorithm.

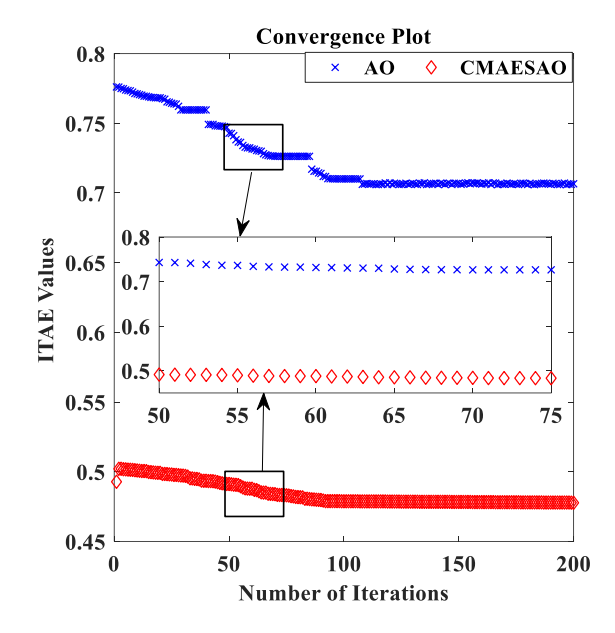


Figure 8. Convergence plot for CMAESAO and AO

6.3. Result analysis

The effectiveness of the proposed D-STATCOMs allocation technique is evaluated by conducting tests on two commonly used distribution systems: a 33-bus system and a 69-bus system. To validate the method's efficacy, three distinct scenarios are examined. In the first scenario, only one D-STATCOM is installed. In the second and third scenarios, two and three D-STATCOMs are respectively considered. The best outcome from ten separate algorithm runs is reported for each scenario. The proposed algorithm is executed on an AMD Ryzen 9 7950X CPU operating at 5.70 GHz with 32 GB of RAM using the MATLAB environment.

6.3.1. 33 bus system

The IEEE 33 bus test system has a combined load of 3715 + j 2300 kVA. The IEEE-33 bus system is subjected to load flow analysis with and without the presence of DSTATCOM. The base case result which is presented in Table 3, shows the poor performance of the system in the absence of D-STATCOM, characterized by a real power loss of 202 kW and a low voltage magnitude of 0.9038 p.u. However, with the inclusion of D-STATCOM(s), there is a significant improvement in the real power loss and voltage profile of the system. Table 3 provides a comparison of different methods for optimal allocation of D-STATCOMs (allocating D-STATCOMs), demonstrating that the proposed approach outperforms than other methods.

Table 4 summarizes the allocation of DSTATCOMs on different types of loads like constant power, constant current, and constant impedance. Here, we find that, for constant power load model, with one D-STATCOM, the power loss is 145.8796 kW, with two D-STATCOMs it is 125.9263 kW, and with three D-STATCOMs it is 124.0499 kW. It shows the improvement of the above system parameters by allocation of two or three DSTATCOMs. For constant current load model, with one D-STATCOM, the power loss is 131.292 kW, with two D-STATCOMs it is 125.9263 kW, and with three D-STATCOMs it is 124.0499 kW. Similarly, for constant impedance load model with one D-STATCOM, the power loss is 119.5428 kW, with two D-STATCOMs it is 116.2869 kW, and with three D-STATCOMs it is 112.7221 kW. So, it can be

concluded that, for each load model, the amount of power loss is decreasing gradually, with the increase in number of D-STATCOMs placement.

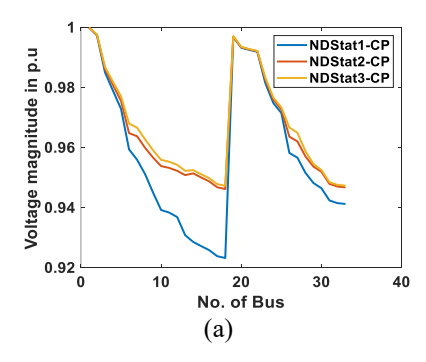
Additionally, Figure 6 shows the convergence characteristic curve of the CMAESAO for distributing D-STATCOMs in the 33-bus system. Based on the results, it can be said that using three D-STATCOM placements results in better system performance than using one or two D-STATCOM allocations. To further support this conclusion, Figures 9(a)-9(c) display the voltage profile, branch current profile, and power loss profile for varying numbers of D-STATCOM allocations and constant power (CP) load types. Figures 10(a)-10(c) display the voltage profile, branch current profile, and power loss profile for varying numbers of D-STATCOM allocations and constant impedance (CI) load types. Figures 11(a)-11(c) display the voltage profile, branch current profile, and power loss profile for varying numbers of D-STATCOM allocations and constant current (CC) load types.

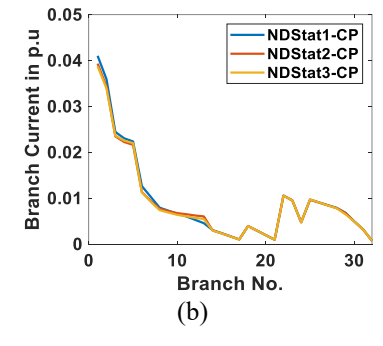
	Table 3.	Effect	of D-	-STAT	COM	allocation	on 33	bus system
--	----------	--------	-------	-------	-----	------------	-------	------------

Methods	N _{Dstatcom}	Location	Size, MVAr	Ploss, kW	Vmin (p.u.)	VSI
Base Case	0	-	-	202.0	0.9038	0.6951
Proposed	1	30	1.0	145.8792	0.9255	0.7266
ĞA	1	12	1.11142	173.9	-	-
IA	1	12	0.9624	171.8	-	-
DE	1	30	1.2527	143.5	0.9256	-
Proposed	2	14	0.5550	125.9263	0.9473	0.8051
		30	1.0			
Proposed	3	30	0.9063	124.0499	0.9495	0.8128
_		16	0.5356			
		7	0.6209			

Table 4. Effect of D-STATCOM allocation on different types of load on 33 bus system

Table 1. Effect of B STITT COM another on afficient types of four on 35 out System										
DSTATCOM	Type of load	Location	Size in MW	Ploss in kW	Qloss in kVar	VSI	Vmin(p.u)			
1	CP	30	1.000	145.8792	97.4253	0.7266	0.9233			
2	CP	14,30	0.5958	125.9263	92.5352	0.8051	0.9473			
			1.000							
3	CP	14,6,30	0.5183	124.0499	91.4507	0.8128	0.9495			
			0.6210							
			0.8098							
1	CC	30	1.000	131.292	87.5134	0.7412	0.9279			
2	CC	14,30	0.5554	125.9263	84.1698	0.8051	0.9473			
			1.000							
3	CC	30,16,7	0.9063	124.0499	83.5563	0.8128	0.9495			
			0.3568							
			0.6209							
1	CI	30	1.000	119.5428	79.548	0.7536	0.9318			
2	CI	30,14	0.9969	116.2869	77.6337	0.8123	0.9494			
			0.5538							
3	CI	24,30,14	0.4421	112.7221	75.1925	0.8066	0.9478			
			0.8978							
			0.5009							





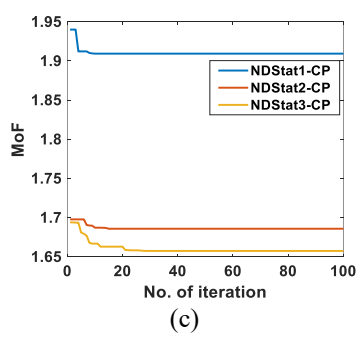


Figure 9. For an IEEE-33 bus system for CP load type: (a) voltage profile, (b) branch current profile, and (c) MoF plot

854 **I**ISSN: 2252-8792

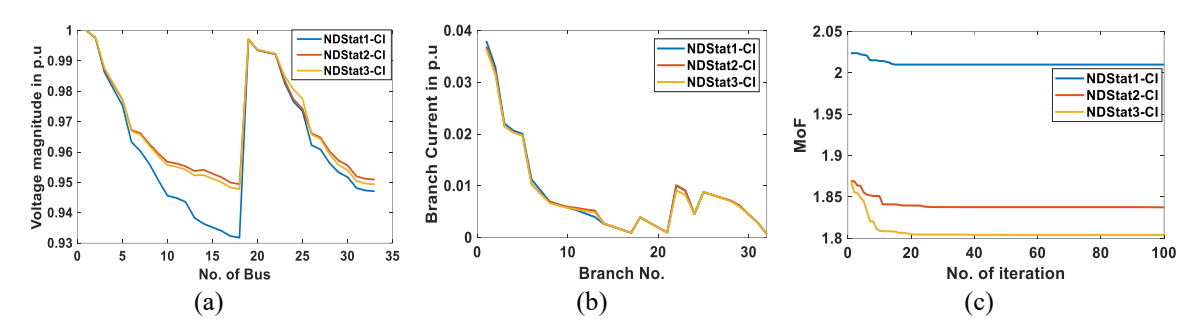


Figure 10. For an IEEE-33 bus system for CI load type: (a) voltage profile, (b) branch current profile, and (c) MoF

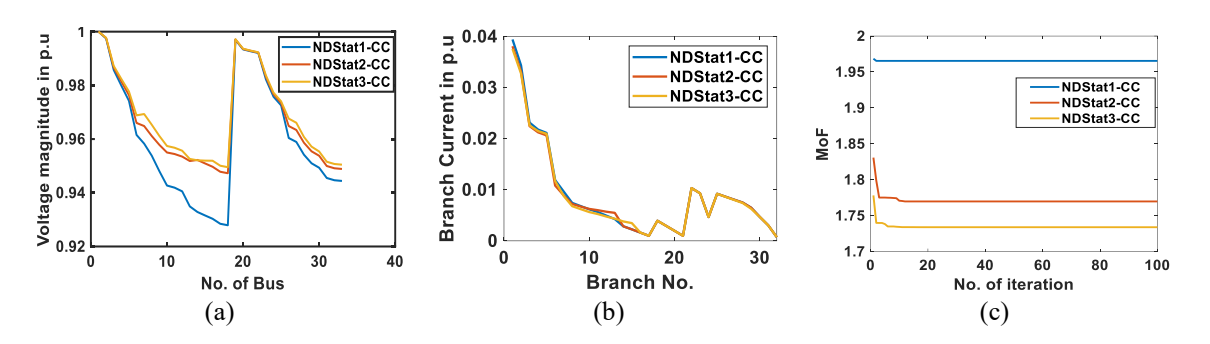


Figure 11. For an IEEE-33 bus system for CC load type: (a) voltage profile, (b) branch current profile, and (c) MoF plot

6.3.2. 69 bus system

The IEEE 33 bus test system has a combined load of $3791.9 + j\ 2694\ kVA$. The IEEE-33 bus system is subjected to load flow analysis with and without the presence of DSTATCOM. The results of which are presented in Table 5. The outcomes in Table 5 evidently specify that the system exhibits inadequate performance in the absence of D-STATCOM, resulting in a real power loss of 224.9 kW, and a low magnitude of voltage is $0.9092\ p.u.$

Table 6 summarizes the allocation on different types of loads like constant power, constant current, and constant impedance. Here, we find that, for constant power load model, with one D-STATCOM, the power loss is 156.7697 kW, with two D-STATCOMs it is 149.6368 kW, and with three D-STATCOMs, it is 147.8951 kW. It shows the improvement of the above system parameters by allocation of two or three DSTATCOMs. For constant current load model, with one D-STATCOM, the power loss is 138.0725 kW, with two D-STATCOMs it is 132.3844 kW, and with three D-STATCOMs it is 130.8476 kW. Similarly, for constant impedance load model with one D-STATCOM, the power loss is 123.242 kW, with two D-STATCOMs, it is 118.3333 kW, and with three D-STATCOMs, it is 118.2958 kW. So, it can be concluded that, for each load model, the amount of power loss is decreasing gradually, with the increase in number of D-STATCOMs placement.

Table 5. Comparison of different methods without and with DSTATCOM allocation on 69 bus system

Methods	$N_{Dstatcom}$	Location	Size, MVAr	Ploss, kW	Vmin (p.u.)	VSI
Base Case	0	-	-	224.9	0.9092	0.6833
Proposed	1	62	1.0	156.7697	0.926	0.7354
PSO	1	61	0.9011	167.9	-	-
GA	1	61	1.9183	165.4	0.9392	-
IA	1	61	1.7044	157.5	-	-
DE	1	61	1.3121	152.0	0.9398	
GSA	1	61	0.966	152.0	-	
Proposed	2	61	1.0	149.6368	0.9286	0.7436
•		12	0.8677			
Proposed	3	62	0.7763	147.8951	0.9338	0.7605
-		18	0.4415			
		61	0.6480			

Table 6. Effect	of DSTA	ΓCOM alloc	ation on diff	erent types of	load on	69 bus systen
DSTATCOM	Location	Size in MW	Ploss in kW	Qloss in kVar	VSI	Vmin (p.u.)
1	62	1.000	156.7697	72.8499	0.7354	0.926
2	61,12	1.000	149.6368	69.2637	0.7436	0.9286
		0.8676				
3	62,18,61	0.7762	147.8951	68.7109	0.7605	0.9338
		0.4414				
		0.6479				
1	62	1.000	138.0725	64.7834	0.751	0.931
2	61,12	0.9914	132.3844	61.8775	0.7579	0.9331
		0.8408				
3	15,61,64	0.5120	130.8476	61.3436	0.7707	0.937
		0.9630				
		0.3266				
1	61	1.000	123.242	58.344	0.7632	0.9347
2	61,13	1.000	118.3333	55.9826	0.7683	0.9363
		0.5806				
3	23,61,64	0.4355	118.2958	56.0025	0.7809	0.9401
		0.7458				

m

Figures 12(a)-12(c) present the performance of the IEEE-69 bus distribution system under CP load conditions for different numbers of D-STATCOMs. The voltage profile in Figure 12(a) shows that integrating one, two, and three D-STATCOMs leads to progressive improvement in maintaining voltage levels close to the nominal value across all buses. Specifically, the minimum voltage magnitude increases significantly, indicating enhanced voltage stability. The branch current profile in Figure 12(b) reveals a corresponding decline in line currents with additional D-STATCOMs, particularly notable in highly loaded branches. Figure 12(c) displays minimization of multi-objective function with simultaneous integration of one, two, and three D-STATCOMs.

0.4976

In Figures 13(a)-13(c), the IEEE-69 bus system is analyzed under CC load conditions. The voltage profile in Figure 11(a) again confirms improved voltage stability with increased D-STATCOM integration, with notable voltage uplift at weaker buses. The branch current profile in Figure 13(b) highlights reductions in line loading, easing thermal stress, and enhancing operational reliability. The power loss plot in Figure 13(c) displays minimization of multi-objective function with simultaneous integration of one, two, and three D-STATCOMs. The loss values are consistently lower when two or more D-STATCOMs are present, confirming the efficiency of optimal placement. Although the improvements between two and three devices are visible, the trade-off in system cost and complexity must be considered, especially when performance gains are incremental.

Figures 14(a)-14(c) illustrate the system response for 69 bus system under CI load conditions. The voltage profile in Figure 14(a) displays a significant uplift in voltage magnitude with the introduction of D-STATCOMs, particularly in the end buses, where voltage drops are usually more pronounced. The branch current profile in Figure 14(b) again shows a systematic decrease in current magnitude throughout the network as the number of D-STATCOMs increases, leading to more balanced load distribution and reduced I²R losses. The power loss plot in Figure 14(c) displays minimization of multi-objective function with simultaneous integration of one, two, and three D-STATCOMs. Collectively, these figures across all load scenarios validate the effectiveness of the proposed CMAESAO method in optimizing both the placement and size of D-STATCOMs. Importantly, they confirm that while three D-STATCOMs yield the best absolute performance, allocating two D-STATCOMs offers the most cost-effective and efficient solution, particularly for the 69-bus system, as demonstrated in Table 6 and supported by the convergence analysis results.

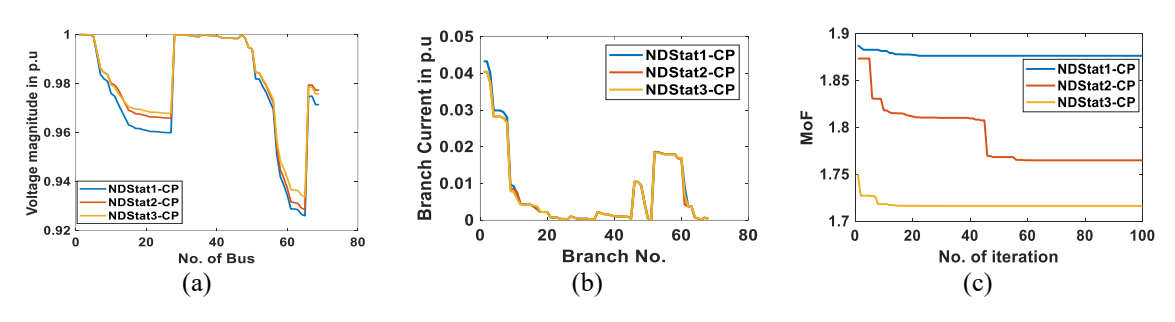


Figure 12. For an IEEE-69 bus system for CP load type: (a) voltage profile, (b) branch current profile, and (c) MoF plot

856 □ ISSN: 2252-8792

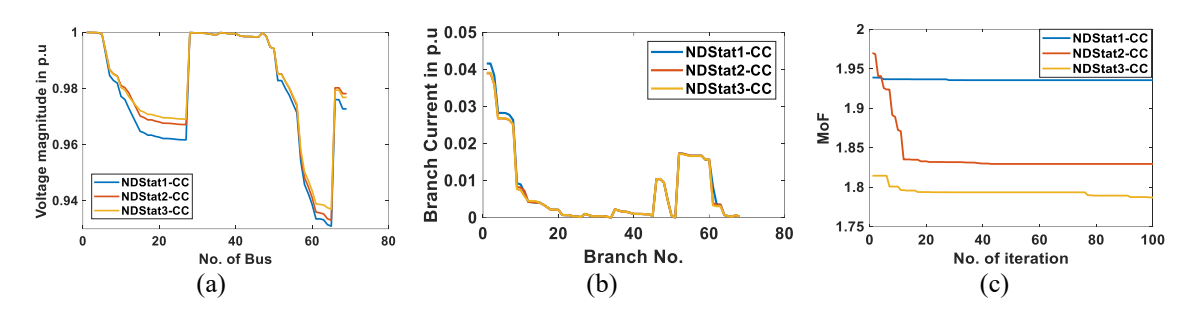


Figure 13. For an IEEE-69 bus system for CC load type: (a) voltage profile, (b) branch current profile, and (c) MoF plot

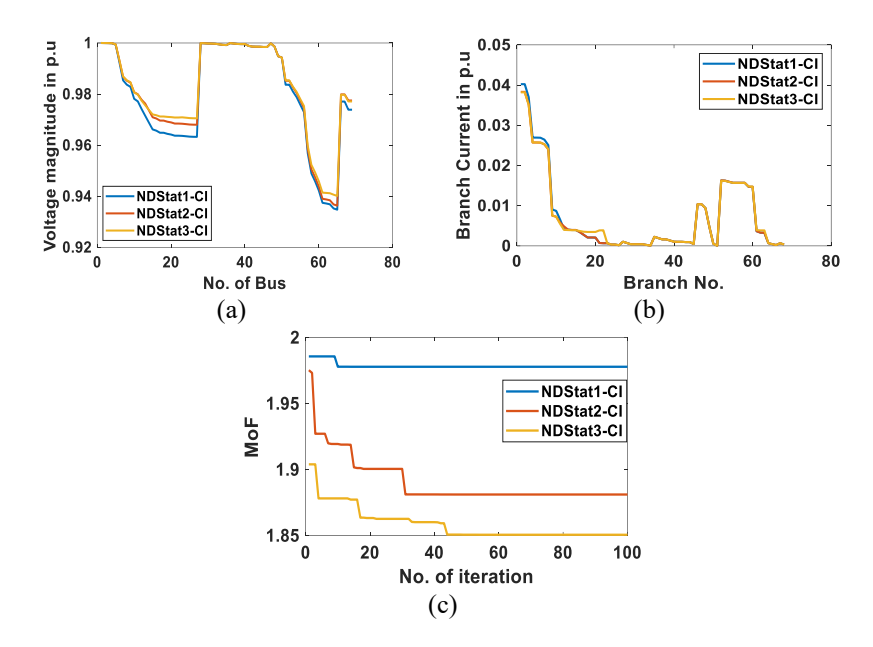


Figure 14. For an IEEE-69 bus system for CI load type: (a) voltage profile, (b) branch current profile, and (c) MoF plot

7. CONCLUSION

Evidently, electrical network reconstruction resulted from in order to minimize power losses in the electrical distribution system and guarantee operational compliance. This study uses the CMAESAO approach to determine the best location and size of D-STATCOM. Two common approaches, the 33-bus system and the 69-bus system, are used to evaluate the method's efficacy. The use of a single D-STATCOM, the deployment of two D-STATCOMs, and the installation of three D-STATCOMs were all evaluated. The analysis's findings show how well the suggested approach works to solve the current issue. Three adequately sized D-STATCOMs were strategically placed in the 33-bus system, which significantly improved the electrical distribution system's performance. However, for the 69-bus system, the implementation of two D-STATCOMs proved superior in reducing power losses compared to the adoption of three D-STATCOMs.

ACKNOWLEDGMENTS

Author thanks to school of electrical engineering, KIIT Deemed to be university, Bhubaneswar, Odisha, India for research guide and help.

FUNDING INFORMATION

This research received no specific grant from any funding agency in the public, commercial, or not-for-profit sectors.

AUTHOR CONTRIBUTIONS STATEMENT

This journal uses the Contributor Roles Taxonomy (CRediT) to recognize individual author contributions, reduce authorship disputes, and facilitate collaboration.

Name of Author	C	M	So	Va	Fo	I	R	D	0	E	Vi	Su	P	Fu
Smrutirekha Mahanta	✓	✓	✓	✓	✓	✓		✓	✓	✓	✓			✓
Manoj Kumar Maharana	\checkmark	\checkmark	✓	\checkmark	\checkmark	\checkmark	✓	\checkmark		\checkmark	✓	\checkmark	\checkmark	\checkmark

C: Conceptualization I: Investigation Vi: Visualization
M: Methodology R: Resources Su: Supervision
So: Software

Fo: Formal analysis E: Writing - Review & Editing

CONFLICT OF INTEREST STATEMENT

The author declares that there is no conflict of interest regarding the publication of this paper.

DATA AVAILABILITY

The data that support the findings of this study are available from the corresponding author upon reasonable request. All simulation results were generated using standard IEEE test systems and can be reproduced with the described methodology.

REFERENCES

- [1] D. Q. Hung, N. Mithulananthan, and R. C. Bansal, "Analytical strategies for renewable distributed generation integration considering energy loss minimization," *Applied Energy*, vol. 105, pp. 75–85, 2013, doi: 10.1016/j.apenergy.2012.12.023.
- [2] S. Devi and M. Geethanjali, "Optimal location and sizing determination of distributed generation and DSTATCOM using particle swarm optimization algorithm," *International Journal of Electrical Power and Energy Systems*, vol. 62, pp. 562–570, 2014, doi: 10.1016/j.ijepes.2014.05.015.
- [3] S. Devi and M. Geethanjali, "Application of modified bacterial foraging optimization algorithm for optimal placement and sizing of distributed generation," Expert Systems with Applications, vol. 41, no. 6, pp. 2772–2781, 2014, doi: 10.1016/j.eswa.2013.10.010.
- [4] A. R. Jordehi, "Allocation of distributed generation units in electric power systems: A review," *Renewable and Sustainable Energy Reviews*, vol. 56, pp. 893–905, 2016, doi: 10.1016/j.rser.2015.11.086.
- [5] B. Das, V. Mukherjee, and D. Das, "DG placement in radial distribution network by symbiotic organisms search algorithm for real power loss minimization," *Applied Soft Computing Journal*, vol. 49, pp. 920–936, 2016, doi: 10.1016/j.asoc.2016.09.015.
- [6] N. Acharya, P. Mahat, and N. Mithulananthan, "An analytical approach for DG allocation in primary distribution network," *International Journal of Electrical Power and Energy Systems*, vol. 28, no. 10, pp. 669–678, 2006, doi: 10.1016/j.ijepes.2006.02.013.
 [7] T. Yuvaraj, K. R. Devabalaji, and K. Ravi, "Optimal allocation of DG in the radial distribution network using bat optimization
- [7] T. Yuvaraj, K. R. Devabalaji, and K. Ravi, "Optimal allocation of DG in the radial distribution network using bat optimization algorithm," in *Lecture Notes in Electrical Engineering*, vol. 436, Springer, Singapore, pp. 563–569, 2017, doi: 10.1007/978-981-10-4394-9 55.
- [8] K. H. Truong, P. Nallagownden, I. Elamvazuthi, and D. N. Vo, "A quasi-oppositional-chaotic symbiotic organisms search algorithm for optimal allocation of DG in radial distribution networks," *Applied Soft Computing Journal*, vol. 88, p. 106067, 2020, doi: 10.1016/j.asoc.2020.106067.
- [9] T. T. Tran, K. H. Truong, and D. N. Vo, "Stochastic fractal search algorithm for reconfiguration of distribution networks with distributed generations," *Ain Shams Engineering Journal*, vol. 11, no. 2, pp. 389–407, 2020, doi: 10.1016/j.asej.2019.08.015.
- [10] C. H. Prasad, K. Subbaramaiah, and P. Sujatha, "Cost-benefit analysis for optimal DG placement in distribution systems by using elephant herding optimization algorithm," *Renewables: Wind, Water, and Solar*, vol. 6, no. 1, pp. 1–12, 2019, doi: 10.1186/s40807-019-0056-9.
- [11] U. Raut, S. Mishra, and D. P. Mishra, "An adaptive NSGA II for optimal insertion of distributed generators in radial distribution systems," in *Proceedings - 2019 International Conference on Information Technology, ICIT 2019*, 2019, pp. 65–69, doi: 10.1109/ICIT48102.2019.00018.
- [12] T. Niknam, A. Kavousifard, S. Tabatabaei, and J. Aghaei, "Optimal operation management of fuel cell/wind/photovoltaic power sources connected to distribution networks," *Journal of Power Sources*, vol. 196, no. 20, pp. 8881–8896, 2011, doi: 10.1016/j.jpowsour.2011.05.081.
- [13] T. Niknam, A. M. Ranjbar, and A. R. Shirani, "Impact of distributed generation on volt/var control in distribution networks," in 2003 IEEE Bologna Power Tech Conference Proceedings, 2003, vol. 3, pp. 210–216, doi: 10.1109/PTC.2003.1304390.
- [14] T. P. Nguyen and D. N. Vo, "A novel stochastic fractal search algorithm for optimal allocation of distributed generators in radial distribution systems," *Applied Soft Computing Journal*, vol. 70, pp. 773–796, 2018, doi: 10.1016/j.asoc.2018.06.020.
- [15] S. Kumar, K. K. Mandal, and N. Chakraborty, "A novel opposition-based tuned-chaotic differential evolution technique for techno-economic analysis by optimal placement of distributed generation," *Engineering Optimization*, vol. 52, no. 2, pp. 303–324, 2020, doi: 10.1080/0305215X.2019.1585832.
- [16] E. S. Ali, S. M. Abd Elazim, and A. Y. Abdelaziz, "Ant lion optimization algorithm for optimal location and sizing of renewable distributed generations," *Renewable Energy*, vol. 101, pp. 1311–1324, 2017.
- [17] M. M. Aman, G. B. Jasmon, A. H. A. Bakar, and H. Mokhlis, "A new approach for optimum simultaneous multi-DG distributed generation Units placement and sizing based on maximization of system loadability using HPSO (hybrid particle swarm optimization) algorithm," *Energy*, vol. 66, pp. 202–215, 2014, doi: 10.1016/j.energy.2013.12.037.

858 🗖 ISSN: 2252-8792

[18] D. R. Prabha and T. Jayabarathi, "Optimal placement and sizing of multiple distributed generating units in distribution networks by invasive weed optimization algorithm," *Ain Shams Engineering Journal*, vol. 7, no. 2, pp. 683–694, 2016, doi: 10.1016/j.asej.2015.05.014.

- [19] D. B. Prakash and C. Lakshminarayana, "Multiple DG placements in radial distribution system for multi objectives using whale optimization algorithm," *Alexandria Engineering Journal*, vol. 57, no. 4, pp. 2797–2806, 2018, doi: 10.1016/j.aej.2017.11.003.
- [20] D. Q. Hung, N. Mithulananthan, and K. Y. Lee, "Optimal placement of dispatchable and nondispatchable renewable DG units in distribution networks for minimizing energy loss," *International Journal of Electrical Power and Energy Systems*, vol. 55, pp. 179– 186, 2014, doi: 10.1016/j.ijepes.2013.09.007.
- [21] J. Siahbalaee, N. Rezanejad, and G. B. Gharehpetian, "Reconfiguration and DG sizing and placement using improved shuffled frog leaping algorithm," *Electric Power Components and Systems*, vol. 47, no. 16–17, pp. 1475–1488, 2019, doi: 10.1080/15325008.2019.1689449.
- [22] U. Raut and S. Mishra, "An improved sine-cosine algorithm for simultaneous network reconfiguration and DG allocation in power distribution systems," *Applied Soft Computing Journal*, vol. 92, pp. 92–106, 2020, doi: 10.1016/j.asoc.2020.106293.
- [23] H. Teimourzadeh and B. Mohammadi-Ivatloo, "A three-dimensional group search optimization approach for simultaneous planning of distributed generation units and distribution network reconfiguration," *Applied Soft Computing*, vol. 88, p. 106012, 2020, doi: 10.1016/j.asoc.2019.106012.
- [24] P. K. Kaushal and M. Tomar, "Real and reactive power loss minimization of IEEE-33 bus by optimal DG placement using LSO in RDS," in 2017 International Conference on Energy, Communication, Data Analytics and Soft Computing (ICECDS), 2017, pp. 1841–1844, doi: 10.1109/ICECDS.2017.8389767.
- [25] A. Alam, B. Zaheer, and M. Zaid, "Optimal placement of DG in distribution system for power loss minimization and voltage profile improvement," in 2018 International Conference on Computing, Power and Communication Technologies (GUCON), 2018, pp. 837–842, doi: 10.1109/GUCON.2018.8674930.
- [26] G. Fandi, I. Ahmad, F. O. Igbinovia, Z. Muller, J. Tlusty, and V. Krepl, "Voltage regulation and power loss minimization in radial distribution systems via reactive power injection and distributed generation unit placement," *Energies*, vol. 11, no. 6, p. 1399, 2018, doi: 10.3390/en11061399.
- [27] S. Angalaeswari, P. Sanjeevikumar, K. Jamuna, and Z. Leonowicz, "Hybrid pipso-sqp algorithm for real power loss minimization in radial distribution systems with optimal placement of distributed generation," *Sustainability*, vol. 12, no. 14, pp. 1–21, 2020, doi: 10.3390/su12145787.
- [28] O. A. Zongo and A. Oonsivilai, "Optimal placement of distributed generator for power loss minimization and voltage stability improvement," Energy Procedia, vol. 138, pp. 134–139, 2017, doi: 10.1016/j.egypro.2017.10.080.
- [29] P. D. P. Reddy, V. C. V. Reddy, and T. G. Manohar, "Whale optimization algorithm for optimal sizing of renewable resources for loss reduction in distribution systems," *Renewables: Wind, Water, and Solar*, vol. 4, no. 1, pp. 1–13, 2017, doi: 10.1186/s40807-017-0040-1.
- [30] A. A. A. El-Ela, R. A. El-Schiemy, and A. S. Abbas, "Optimal placement and sizing of distributed generation and capacitor banks in distribution systems using water cycle algorithm," *IEEE Systems Journal*, vol. 12, no. 4, pp. 3629–3636, 2018, doi: 10.1109/JSYST.2018.2796847.
- [31] P. P. Biswas, R. Mallipeddi, P. N. Suganthan, and G. A. J. Amaratunga, "A multiobjective approach for optimal placement and sizing of distributed generators and capacitors in distribution network," *Applied Soft Computing Journal*, vol. 60, pp. 268–280, 2017, doi: 10.1016/j.asoc.2017.07.004.
- [32] P. D. P. Reddy, V. C. V. Reddy, T. G. Manohar, "Ant lion optimization algorithm for optimal sizing of renewable energy resources for loss reduction in distribution systems," *Journal of Electrical Systems and Information Technology*, vol. 5, no. 3, pp. 663-680, 2018, doi: 10.1016/j.jesit.2017.06.001.
- [33] S. Essallah, A. Bouallegue, and A. Khedher, "Optimal sizing and placement of DG units in radial distribution system," *International Journal of Renewable Energy Research (IJRER)*, vol. 8, no. 1, pp. 166–177, 2018.

BIOGRAPHIES OF AUTHORS



Smrutirekha Mahanta is a Ph.D. scholar in Kalinga Institute of Industrial Technology (KIIT), Deemed to be University, Odisha, India. She is doing research in the field of integration of DG to grid. She received her master degree from IIT, Kharagpur in the year of 2015 in electrical engineering. She is a certified master trainer of solar PV installer Suryamitra from SCGJ and master trainer of didactics and enhance teaching methods from RENAC Germany. She can be contacted at email: m.smrutirekha88@gmail.com.



Manoj Kumar Maharana working as associate professor at Kalinga Institute of Industrial Technology (KIIT), Bhubaneswar, India since 2011 till date. He completed his doctorate degree in electrical engineering from IIT Madras in 2010. He has completed his master degree from REC (NIT) Warangal, Andhra Pradesh in 2001 in power system specialization. He has teaching and research experience of more than 20 years in the field of electrical engineering. His main area of interest in research is power system operation and control. He can be contacted at email: mkmfel@kiit.ac.in.